NANO LETTERS

Letter

pubs.acs.org/NanoLett

Three-Dimensional Spirals of Atomic Layered MoS_2

Liming Zhang,[†] Kaihui Liu,[‡,§] Andrew Barnabas Wong,[†,∥] Jonghwan Kim,[‡] Xiaoping Hong,[‡] Chong Liu,[†,∥] Ting Cao,[‡] Steven G. Louie,[‡,∥] Feng Wang,*[,‡,∥,⊥] and Peidong Yang*[,†,∥,⊥,#]

[†]Department of Chemistry and [‡]Department of Physics, University of California at Berkeley, Berkeley, California 94720, United States

[§]State Key Laboratory for Mesoscopic Physics and Collaborative Innovation Centre of Quantum Matter, Peking University, Beijing 100871, China

[∥]Materials Sciences Division, Lawrence Berkeley National Laboratory, Berkeley, California 94720, United States

[⊥]Kavli Energy NanoSciences Institute at the University of California, Berkeley and the Lawrence Berkeley National Laboratory, Berkeley, California 94720, United States

[#]Department of Material Science and Engineering, University of California at Berkeley, Berkeley, California 94720, United States

Supporting Information

ABSTRACT: Atomically thin two-dimensional (2D) layered materials, including graphene, boron nitride, and transition metal dichalcogenides (TMDs), can exhibit novel phenomena distinct from their bulk counterparts and hold great promise for novel electronic and optoelectronic applications. Controlled growth of such 2D materials with different thickness, composition, and symmetry are of central importance to realize their potential. In particular, the ability to control the symmetry of TMD layers is highly desirable because breaking the inversion symmetry can lead to intriguing valley physics, nonlinear optical properties, and piezoelectric responses. Here we report the first chemical vapor deposition (CVD) growth of spirals of layered MoS_2 with atomically thin helical periodicity, which exhibits a chiral structure and breaks the three-dimensional (3D) inversion symmetry explicitly. The spirals composed of tens of connected MoS_2 layers with decreasing areas: each basal plane has a triangular shape and shrinks gradually to the summit when spiraling up. All the layers in the spiral assume an AA lattice stacking, which is in contrast to the centrosymmetric AB stacking in natural MoS_2 crystals. We show that the noncentrosymmetric MoS_2 spiral leads to a strong bulk second-order optical nonlinearity. In addition, we found that the growth of spirals involves a dislocation mechanism, which can be generally applicable to other 2D TMD materials.

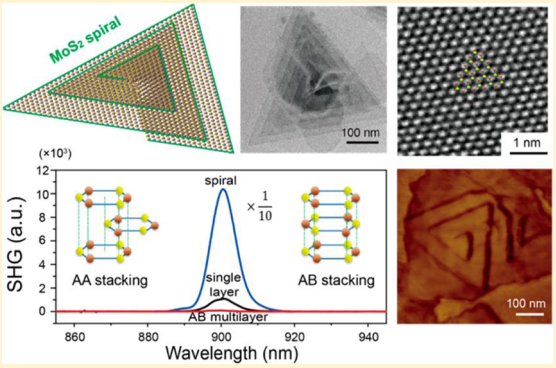

KEYWORDS: *Molybdenum disulfide (MoS_2), spirals, symmetry breaking, chemical vapor deposition, screw dislocation*

Transition metal dichalcoginides (TMDs), a family of atomically thin 2D materials, have attracted much research interest due to their novel layer-dependent electronic and optical properties.[1−10] For instance, monolayer MoS_2 exhibits a direct optical bandgap of ∼1.8 eV in the visible range,[3,4] an exciton binding energy of a large fraction of ∼1 eV,[10] an emerging valley degree of freedom,[11−13] and a strong second-order optical nonlinearity,[14] which are promising for novel applications ranging from nanoelectronics[7] and photonics[8] to photovoltaics[9] and valleytronics.[11−13] Many of the intriguing properties of monolayer MoS_2, such as valley polarizations and the second order nonlinearity, originate from its noncentrosymmetric structure compared with centrosymmetric bilayers or bulk MoS_2. Many other physical properties, such as piezoelectric responses and Pockels effects, also emerge only when the inversion symmetry is broken.[15] To better explore the effect of symmetry in layered TMDs, it is highly desirable to synthesize TMD structures with controlled symmetry properties. The spiral is an intriguing structure that can be found in nature and artificial materials. Spiral structures are chiral and automatically break the reflection and inversion symmetry. Previously nanoscale spirals have been realized in nanoplates,[16−18] nanotubes,[19] and Eshelby twisted nanowires.[20,21] Here we show that spirals of atomic-layered MoS_2 involving screw dislocations can also be grown directly using chemical vapor deposition (CVD), and these MoS_2 spirals exhibit interesting physical properties.

Large-sized highly crystalline MoS_2 monolayer was successfully grown by CVD method recently.[22−24] To grow the atomic layered spiral structures, we developed an approach based on these previous methods but with modified growth conditions (See Methods and Supporting Information S1). Our key control is to increase the nucleation rate at the initial stage to

Received: August 1, 2014
Revised: October 2, 2014
Published: October 24, 2014

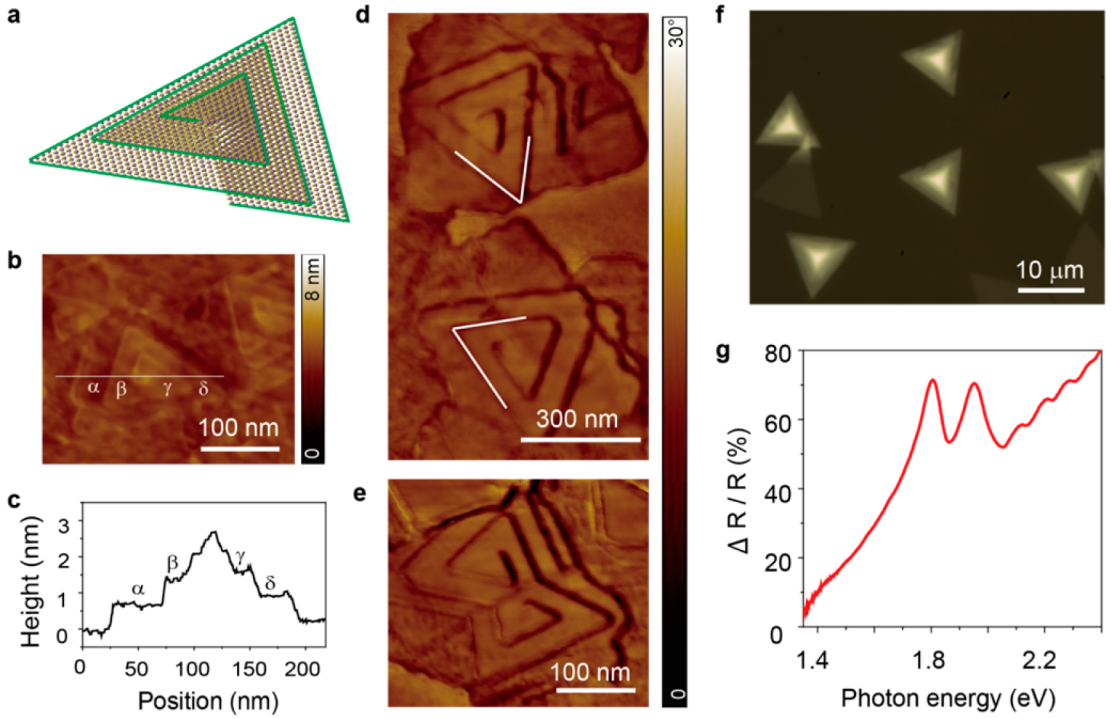

Figure 1. Morphology of atomic layered MoS_2 spirals. (a) Schematic illustration of the MoS_2 spiral. (b,c) AFM image (height signal) of 300 nm large (defined as the length of bottom triangle) spiral. The profile (c) is taken along the white line in (b), showing obvious plateaus (marked by α, β, γ, and δ) with step height of about 0.62 nm. (d) AFM image (phase signal) of MoS_2 spirals with left (upper) and right (lower) handedness. (e) AFM image (phase signal) of MoS_2 spiral with two screws inside, exhibiting twinlike structure. (f) Bright-field optical image of ~10 μm sized spirals. They overall look like pyramids; each basal plane has a triangular shape and shrinks gradually to the summit point. (g) Reflection spectrum of spiral on fused silica substrate.

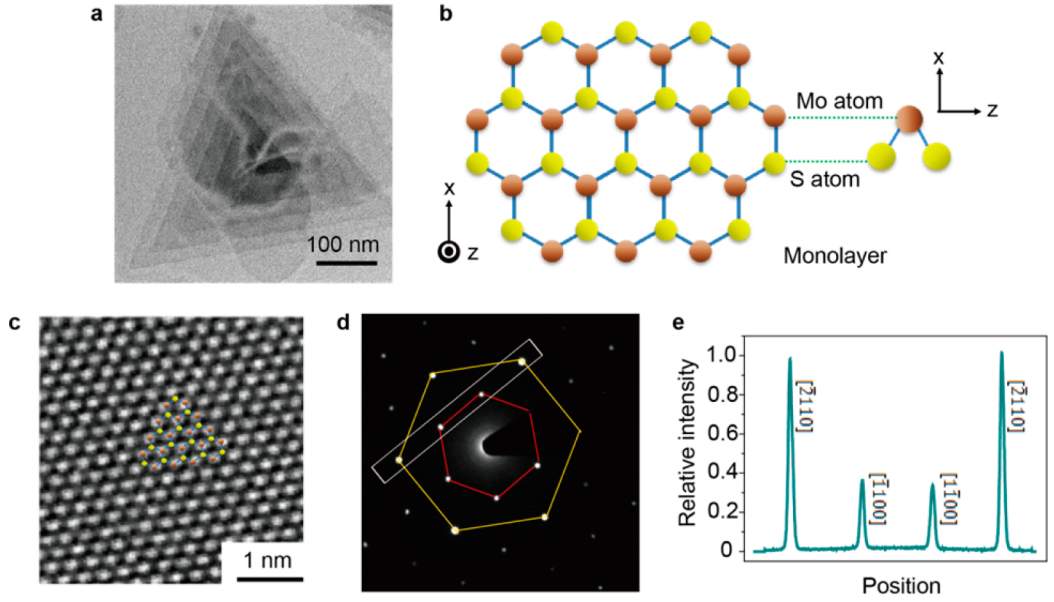

Figure 2. Crystal structure of atomic layered MoS_2 spiral. (a) Representative TEM image from one MoS_2 spiral. It shows clear spiral features: the triangles spiral up layer by layer to the center summit. (b) Top view of monolayer 2D hexagonal lattice structure and side view of a unit cell of the MoS_2 lattice structure. (c,d) HRTEM image (c) and SAED pattern (d) obtained in the center of the MoS_2 spiral in (a). The same trigonal symmetry as in monolayer indicates that the spiral layers are of same lattice structure. (e) Intensity profiles taken along the dashed white box in (d). The intensity profile is different from that in monolayer indicates that the spiral layers have a well-defined stacking order.

generate a dislocation center with high spiraling-up activity. We can grow spiral structures on various substrates, including SiO_2/Si, mica, fused silica, and TiO_2 with yield as high as 80% (the other 20% are mainly monolayers).

The morphology of our spiral structures was characterized by atomic force microscopy (AFM). Figure 1a shows an illustration of the 3D spiral structure, and Figure 1b–e shows the AFM images of several spirals grown on fused silica with size around 300 nm (defined by the edge length of the largest

dx.doi.org/10.1021/nl502961e | Nano Lett. 2014, 14, 6418–6423

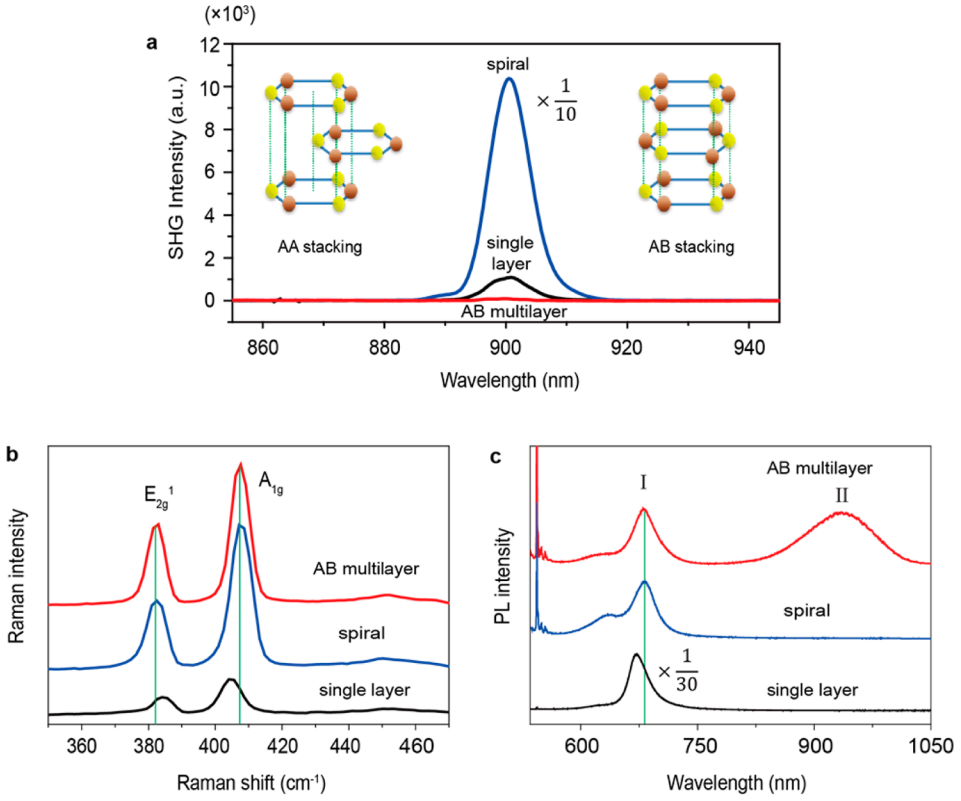

Figure 3. Stacking and interlayer coupling in atomic layered MoS_2 spiral. (a) Nonlinear optical second-harmonic generation (SHG) signal from monolayer, exfoliated AB stacked multilayer and AA stacked spiral of MoS_2. Insets show the side view of AA and AB stacked multilayer lattice, respectively. (b) The Raman spectra in the range of 350−470 cm^{-1} from monolayer, AB stacked multilayer, and spiral, showing the $E_{2g}{}^1$ and A_{1g} modes. The spectra are displaced along the vertical axis for clarity. (c) PL spectra for monolayer, AB stacked multilayer, and spiral. The PL spectra have been displaced along the vertical axis for clarity.

basal plane). The height images (Figure 1b,c) show obvious plateaus with step height of about 0.62 nm, which matches the thickness of single MoS_2 atomic layer.[25] The layer thickness of 0.62 nm could also be independently determined by the X-ray diffraction (XRD) technique (Supporting Information S2). The spirals can be either left or right-handed (Figure 1d) with equal probability. When the spiral density is high, twin- or mirror twinlike spiral structures can be found (Figure 1e). The size of the spirals can be tuned in the range of about 100 nm to 20 μm by the growing conditions. Shown in Figure 1f is a typical bright-field optical image of large-sized spirals (~10 μm). They overall look like pyramids; each basal plane has a triangular shape and shrinks gradually to the summit point. The AFM images of large spirals (Supporting Information S3) show that these "pyramids" have tens of spiral layers.

To confirm the atomic layered spirals originate from MoS_2 layers, we first carried out reflection spectroscopic measurements on fused silica. The reflection spectrum (Figure 1g) shows two prominent peaks at 1.80 and 1.95 eV, in accordance with the two fingerprint exciton transitions in MoS_2.[3] X-ray photoelectron spectroscopy (XPS) was also used to study the elemental composition of spirals (Supporting Information S4). It shows four obvious peaks at 229.0, 232.1, 162.2, and 163.4 eV, which can be attributed to the doublet of Mo $3d_{5/2}$ and $3d_{3/2}$, S $2p_{3/2}$ and $2p_{1/2}$ in MoS_2, respectively.[26]

In order to gain microscopic structure information on the MoS_2 spirals, we employed transmission electron microscopy (TEM) to study the crystal structure of spirals transferred onto TEM grids (see Methods for transfer procedure). Figure 2a shows one typical TEM image of a 300 nm-sized MoS_2 spiral. Clear spiral features as in the AFM images can be identified; the triangles spiral up layer by layer to the center summit. Microscopically, a monolayer MoS_2 consists of two triangle lattices of S atoms and a sheet of Mo atoms occupying trigonal prismatic sites between the S sheets,[27] which forms a hexagonal structure with Mo and S atoms when projected onto the 2D basal plane (Figure 2b). However, high-resolution TEM (HRTEM) images and diffraction patterns of monolayer MoS_2 typically show trigonal lattice structures.[22−24] Our spiral structures here exhibit similar features as that in monolayer MoS_2. The HRTEM image (Figure 2c) taken at the center of the spiral in Figure 2a shows a trigonal lattice with the distance of adjacent bright spots equal to the in-plane Mo−Mo distance of 3.15 Å. The selected area electron diffraction (SAED) taken from the same region shows a single set of pattern characteristic of trigonal structures (Figure 2d), indicating that different spiral layers are of the same crystal orientation. However, the intensity ratio between the $[\bar{2}\ 1\ 1\ 0]$ and $[1\ \bar{1}\ 0\ 0]$ diffraction points is about 2.5, which is quite different from 1.1 as observed in monolayers.[23] It suggests that the adjacent spiral layers have a displacement similar to that in Bernal stacked bilayer graphene.[28]

Two possible MoS_2 stacking orders are compatible with the lattice pattern observed in the HRTEM (Figure 2c) and electron diffraction (Figure 2d). These two stacking orders, referred to as AB and AA stacking, are illustrated in the inset of Figure 3a. For AB stacking, the in-plane Mo−S bond directions are opposite for the two adjacent layers and the crystal structure

dx.doi.org/10.1021/nl502961e | Nano Lett. 2014, 14, 6418−6423

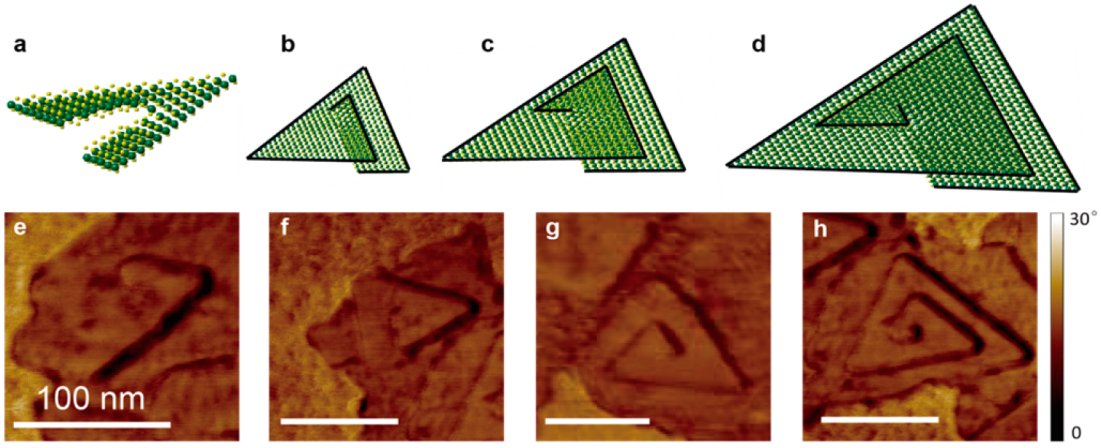

Figure 4. Growing mechanism of atomic layered MoS_2 spiral. (a–d) Schematic illustration of MoS_2 spiral from nucleation to growth. Black lines indicate the exposed edges. (e–h) AFM images (phase signal) of several typical spirals at different growth stages. The growth will start from a slipped edge (e) and generate a small spiraled triangle (f). With growth continued, the generated dislocation core will keep spiraling up vertically and form pyramid-shaped 3D large spirals (g,h).

belongs to the centrosymmetric D^1_{3d} group. The AA stacked MoS_2, however, have the in-plane Mo–S bonds pointing to the same direction in adjacent layers, and it belongs to the noncentrosymmetric D^1_{3h} group. Theoretical calculations based on local-density approximation (LDA) show that the AA and AB stacked MoS_2 are both stable configurations with very similar total energy (For AA stacking order, the staggered stacking configuration is energetically more favorable than the eclipsed configuration. See Supporting Information S5 for details). Natural MoS_2 crystals usually assume the AB-stacked centrosymmetric configuration. For our CVD-grown MoS_2 spirals, all layers show triangular shapes with parallel edges (Figures 1b,d and 2a). Because MoS_2 layers are known to have Mo-terminated zigzag edges,[29] the same triangular orientation in different layers indicates that our MoS_2 spirals are composed of helical layers with AA stacking order. Such AA stacking explicitly breaks the inversion symmetry that presents in bulk MoS_2 crystals, and it can lead to dramatic changes in symmetry-dependent properties of MoS_2 ranging from optical nonlinearity and electro-optics to piezoelectric and valley physics.

Here we examine the second-order optical nonlinearity in the MoS_2 spirals using optical second-harmonic generation (SHG). The SHG signal is extremely sensitive to the symmetry, and it vanishes for any material with inversion symmetry (within the dipole approximation).[14] For MoS_2, it has been demonstrated that the noncentrosymmetric monolayer exhibits strong SHG signals (black curve in Figure 3a) but the centrosymmetric AB stacked bilayer has no SHG due to destructive interference between the signals from the two layers. In fact, the SHG signal from a thick exfoliated AB-stacked MoS_2 crystal is much weaker than that of a monolayer due to the centrosymmetric AB stacking (red curve in Figure 3a).[14] For AA stacked MoS_2, which breaks the inversion center, the SHG signal can increase dramatically with the layer thickness because the signals from different layers interfere constructively with each other. Approximately, SHG should scale as N^2 for MoS_2 thin layers, where N is the MoS_2 layer number.[30] Indeed our spiral structures show very strong SHG (blue curve in Figure 3a). For 6 μm-sized spirals (with a layer number ~15), the SHG signal is almost 2 orders of magnitude higher than that of a MoS_2 monolayer, which is in striking contrast to AB-stacked multilayers (red curve in Figure 3a). This remarkably strong SHG in MoS_2 spirals confirms unambiguously that the different layers are indeed AA stacked with broken inversion symmetry.

Next, we examine the vibrational properties of the AA-stacked MoS_2 spirals using Raman spectroscopy. The Raman spectra in the range of 350–470 cm^{-1} from MoS_2 monolayers, AB-stacked multilayers, and the AA-stacked spirals were compared in Figure 3b. The two prominent Raman peaks around 383 and 407 cm^{-1} correspond to the in-plane $E_{2g}{}^1$ and out-of-plane A_{1g} vibrational modes, respectively. It has been established that the interlayer van der Waals coupling in AB stacked multilayer can soften the $E_{2g}{}^1$ mode and stiffen the A_{1g} mode compared with that in a monolayer.[31] The same trend is observed in AA-stacked MoS_2 spirals, which indicates that the layers in a spiral have comparable mechanical coupling as those in AB-stacked multilayers.

We further explored the photoluminescence (PL) properties of the MoS_2 spirals. Figure 3c shows typical PL spectra from MoS_2 monolayers, AB stacked multilayers, and spirals. The relatively sharp peak I around 670 nm originates from the lowest-energy exciton transition of MoS_2. Monolayer MoS_2 is a direct bandgap material and therefore has very strong PL emission. On the other hand, AB-stacked multilayer MoS_2 has an indirect bandgap. This leads to a strongly reduced PL at peak I (about 1/30 of that in a monolayer), and creates a new PL peak II at 950 nm due to the indirect exciton transition. (The small red shift of peak I can be attributed to the interlayer coupling[3,4]). For spiral structures, the PL of peak I is as weak as that in AB stacked multilayer. Our theoretical calculations show that AA-stacked MoS_2 layers also have an indirect bandgap (Supporting Information S6). However, it is quite unusual that peak II nearly disappears. We tentatively attribute this behavior to the nonradiative recombination of excitons (electron–hole pair) at the extensive metallic edges present in the spiral samples.[31,32]

Finally, we investigate the growth mechanism for atomic-layered MoS_2 spirals. According to Burton–Cabrera–Frank (BCF) theory,[33] screw dislocations can lead to the growth of spiral structures.[16,19–21] The screw dislocation is highly strained and locates at the center of the spiral structures. The formation of a screw dislocation core in MoS_2 spirals requires the generation of slipped planes (screw defects) in the bottom layer (shown in Figure 4a), otherwise the growth will follow an in-

dx.doi.org/10.1021/nl502961e | Nano Lett. 2014, 14, 6418–6423

plane-growth mode and produce monolayers of MoS_2.[22−24] In our refined CVD growth conditions, the seeding of the screw defects was achieved by introducing a spike in supersaturation of sulfur at the initial stage of the reaction. The higher partial pressure of sulfur greatly increases the volatilization speed of MoO_3, forming a large amount of gaseous intermediate MoO_{3-x} in a short time. The higher partial pressure of MoO_{3-x} leads to the higher possibility of accidental overgrowth of two exposed edges, which can lead to a slipped edge with a screw defect (Figure 4a). Once a screw dislocation is created, it will remain active and gradually grow in the vertical direction because continued growth at the edge sites of the dislocation center is energetically favorable. The exposing edges continue to grow with the preference to form a triangular corner on each step monolayer (turning 120° each time and exposing the low energy Mo−Mo zigzag edge out[29]). Because the upper layer is formed later and has shorter time to grow, the pyramid-shaped 3D atomic layered MoS_2 spiral will be created (Figure 4b−d). Some clues of this growth mechanism can be found from the AFM images taken at different growth stages (Figure 4e−h). Similar to our schematic model, the spiral will grow from a slipped edge (Figure 4e) and generate a small spiraled triangle (Figure 4f). The generated dislocation core will keep spiraling up and form a pyramid-shaped 3D large spiral finally (Figure 4g,h). We note that the bottom layer is not perfectly triangular, likely due to fast nonequilibrium growth conditions at the initial stage. Newly generated layers from a dislocation can grow on top of the bottom layer. On top of these spirals, the dislocation core can be clearly identified.

The MoS_2 spirals are the product of both screw-dislocation driven growth of the core along the vertical dimension and triangular layer expansion along the lateral dimension. The elementary Burgers vector of the screw dislocations in the layered MoS_2 is just one unit cell. Because the upper layers are formed later and have shorter time to grow, the lateral layer size decrease with the height and the spiral forms overall pyramid-like shape. The pyramid slope is determined by the growth velocity ratio between the vertical dislocation growth and lateral monolayer expansion. Because a large strain is present at the dislocation core, the vertical growth is significantly slower than the lateral expansion. Typically we found the in-plane monolayer growth rate is 50−100 times faster than the vertical nucleation center for 300 nm spirals and 300−500 times for 20 μm spirals. The larger ratio in bigger spiral is presumably due to the decreased supersaturation over time in our growth condition (Supporting Information S1). We believe that this mechanism of spiral growth is not limited to MoS_2. Many other 2D atomic layered materials with strong in-plane covalent bonding and weak out-of-plane van der Waals interaction, such as WS_2, $MoSe_2$, and WSe_2, share similar CVD growth mechanism. Therefore, systematical optimizing the growth conditions will create a family of spiraled 2D layers of TMDs.

In summary, we grow and characterize spiral structure of atomic layered MoS_2 grown by CVD for the first time. These noncentrosymmetric TMD spirals, in contrary to their centrosymmetric bulk crystals, can lead to new behavior in electro-optic, piezoelectric, and nonlinear optical responses as well as valley physics, which may find applications in nanoscale electronic and optical devices.

Methods. *Growth of Atomic Layered MoS_2 Spirals.* We grew MoS_2 spirals by CVD on various substrates using MoO_3 and S powder as precursors. The substrate was loaded into the 1 in. CVD furnace and placed face-down above one crucible containing 5.0−7.5 mg of MoO_3 (≥99.5%, sigma-Aldrich) with another crucible containing 140 mg of S (≥99.5%, sigma-Aldrich). The key difference between the growth of spirals and monolayer MoS_2 is the location temperature regions of S. In order to increase the possibility to get spirals, S was loaded in the high-temperature region close to MoO_3. The CVD process was performed under ambient pressure while flowing ultrahigh-purity nitrogen. The recipe is sit 1 h at 105 °C with 500 sccm, ramp to 700 °C at 15 °C/min with 10−15 sccm N_2, sit 5 min at 700 °C, and cool down naturally with 500 sccm gas flow. The domain size of MoS_2 spirals could be tuned from several hundreds of nanometers to tens of micrometers depending on growth conditions. More detailed information on the growth of spirals can be found in the Supporting Information S1.

Preparation of Monolayer and AB-Stacked Multilayer MoS_2. For monolayer MoS_2 growth, the substrate was loaded above one crucible containing 20 mg of MoO_3 together with another crucible containing 6.5−7.0 mg of S and the distance between S and MoO_3 is about 12 cm. The CVD process was performed under ambient pressure while flowing ultrahigh-purity nitrogen. The recipe is sit 1 h at 105 °C with 500 sccm, ramp to 650 °C at 15 °C/min with 10 sccm N_2, sit 5 min at 650 °C, and cool down naturally with 500 sccm gas flow. AB-stacked multilayer MoS_2 was mechanically exfoliated from bulk crystal of 2H-MoS_2 (SPI, natural molybdenite) and identified by optical microscope.

Sample Characterization. (1) Atomic force microscope (Veeco Nanoscope) in tapping mode was used for morphology studies of MoS_2 spirals.

(2) TEM images and electron diffraction patters were taken by JEOL 2100 at an accelerating voltage of 200 kV. TEM samples were transferred from the as-grown substrate and procedure is shown below. Polymer transfer layers were prepared by spin-coating poly(methyl methacrylate) (PMMA) A4 onto fused silica chips (MoS_2 side) at 3000 rpm for 60 s to form ∼200 nm thick layer. The chips were floated on HF aqueous solution (10 wt %) for several hours. The HF etched fused silica slowly, causing the chips to fall off and leaving the MoS_2-coated PMMA film floating on the solution surface. The membrane was transferred to deionized water two times and then scooped onto TEM grid and dried. The PMMA film was removed by baking the TEM grid at 350 °C in N_2/H_2 gas (500/20 sccm) flow for 2 h at atmospheric pressure.

(3) Reflection spectra were taken by our home-built system. A supercontinuum laser (470−1800 nm) is used as the light source. We focus the supercontinuum down to ∼2 μm and analyze the signal with a spectrograph equipped with an array charged coupled device (CCD) detector. Two sets of reflection spectra with the MoS_2 spiral inside beam (I_{inside}) and outside beam ($I_{outside}$) are taken and the final spectrum is obtained as $\Delta R/R = (I_{inside} - I_{outside})/I_{outside}$.

(4) SHG signal were taken by our home-built setup. We use femtosecond pulses with 1.8 μm wavelength and 250 fs pulse width, which is generated by an optical parametric amplifier (OPA). OPA is pumped by femtosecond pulses at 1026 nm (at a repetition rate of 100 kHz) from a regenerative amplifier seeded by a mode-locked oscillator (Light Conversion PHAROS). SHG signal with 900 nm wavelength was collected in the back scattering geometry via confocal microscope and analyzed by a monochromator equipped with liquid nitrogen cooled CCD. Beam size of fundamental light is ∼2 μm and fluence is ∼25 mJ/cm^2.

dx.doi.org/10.1021/nl502961e | Nano Lett. 2014, 14, 6418−6423

(5) Raman spectroscopy and photoluminescence were taken by a Horiba HR800 system with laser excitation energy of 532 nm. The laser spot size is ~1 μm and a laser power of ~5 mW was used to avoid heating and PL saturation.

(6) XPS measurements were carried out using a Kratos Axis Ultra spectrometer with Al kα monochromated X-ray at low pressures of 5×10^{-9} to 1×10^{-8} Torr. The collection area was about 300 × 700 μm^2. The highest peak in C 1s spectra was shifted to 284.8 eV for charge correction.

■ ASSOCIATED CONTENT

Supporting Information

Detailed information for CVD synthesis, XRD, AFM, and XPS characterization of MoS_2 spirals; theoretical calculation on the stacking stability and band structure of AA stacked MoS_2. This material is available free of charge via the Internet at http://pubs.acs.org.

■ AUTHOR INFORMATION

Corresponding Authors

*E-mail: (P.Y.) p_yang@berkeley.edu.

*E-mail: (F.W.)fengwang76@berkeley.edu.

Author Contributions

P.D.Y., F.W., L.M.Z., and K.H.L. conceived the experiments. L.M.Z. developed and performed the synthesis experiment. L.M.Z., K.H.L., A.B.W. and C.L. performed the material structural and spectroscopic characterization. J.K. and X.P.H. contributed to the nonlinear optical measurement. S.G.L. and T.C. performed theoretical calculation and interpretation. F.W., L.M.Z., K.H.L., J.K. and X.P.H. performed data analysis. P.D.Y., F.W., L.M.Z. and K.H.L. cowrote the manuscript. All authors discussed the results and commented on the paper.

Author Contributions

L.Z. and K.L. contributed equally.

Notes

The authors declare no competing financial interest.

■ ACKNOWLEDGMENTS

This work was supported by the Director, Office of Science, Office of Basic Energy Sciences, Materials Sciences and Engineering Division, of the U.S. Department of Energy under Contract No. DE-AC02-05CH11231(P-Chem) and No. DE-SC0003949 (Early Career Award). We thank the Molecular Foundry and Lawrence Berkeley National Laboratory for use of their facilities. We would especially like to thank Professor William Nix at Stanford University for the help discussion on the formation mechanism of spirals. K.L. acknowledges support from National Program for Thousand Young Talents of China.

■ REFERENCES

(1) Novoselov, K. S.; Geim, A. K.; Morozov, S. V.; Jiang, D.; Katsnelson, M. I.; Grigorieva, I. V.; Dubonos, S. V.; Firsov, A. A. *Nature* **2005**, *438*, 197−200.

(2) Zhang, Y. B.; Tan, Y. W.; Stormer, H. L.; Kim, P. *Nature* **2005**, *438*, 201−204.

(3) Mak, K. F.; Lee, C.; Hone, J.; Shan, J.; Heinz, T. F. *Phys. Rev. Lett.* **2010**, *105*, 136805.

(4) Splendiani, A.; Sun, L.; Zhang, Y.; Li, T.; Kim, J.; Chim, C. Y.; Galli, G.; Wang, F. *Nano Lett.* **2010**, *10*, 1271−1275.

(5) Bonaccorso, F.; Sun, Z.; Hasan, T.; Ferrari, A. C. *Nat. Photonics* **2010**, *4*, 611−622.

(6) Dean, C.; Young, A.; Meric, I.; Lee, C.; Wang, L.; Sorgenfrei, S.; Watanabe, K.; Taniguchi, T.; Kim, P.; Shepard, K. *Nat. Nanotechnol.* **2010**, *5*, 722−726.

(7) Radisavljevic, B.; Radenovic, A.; Brivio, J.; Giacometti, V.; Kis, A. *Nat. Nanotechnol.* **2011**, *6*, 147−150.

(8) Lopez-Sanchez, O.; Lembke, D.; Kayci, M.; Radenovic, A.; Kis, A. *Nat. Nanotechnol.* **2013**, *8*, 497−501.

(9) Feng, J.; Qian, X. F.; Huang, C. W.; Li, J. *Nat. Photonics* **2012**, *6*, 865−871.

(10) Qiu, D. Y.; Felipe, H.; Louie, S. G. *Phys. Rev. Lett.* **2013**, *111*, 216805.

(11) Mak, K. F.; He, K. L.; Shan, J.; Heinz, T. F. *Nat. Nanotechnol.* **2012**, *7*, 494−498.

(12) Zeng, H. L.; Dai, J. F.; Yao, W.; Xiao, D.; Cui, X. D. *Nat. Nanotechnol.* **2012**, *7*, 490−493.

(13) Cao, T.; Wang, G.; Han, W.; Ye, H.; Zhu, C.; Shi, J.; Niu, Q.; Tan, P.; Wang, E.; Liu, B.; Feng, J. *Nat. Commun.* **2012**, *3*, 887.

(14) Li, Y.; Rao, Y.; Mak, K.; You, Y.; Wang, S.; Dean, C.; Heinz, T. F. *Nano Lett.* **2013**, *13*, 3329−3333.

(15) Duerloo, K.-A. N.; Ong, M. T.; Reed, E. J. *J. Phys. Chem. Lett.* **2012**, *3*, 2871−2876.

(16) Morin, S. A.; Forticaux, A.; Bierman, M. J.; Jin, S. *Nano Lett.* **2011**, *11*, 4449−4455.

(17) Lieth, R. M. A. *Preparation and Crystal Growth of Materials with Layered Structures*; Springer Science+Business Media: New York, 1977.

(18) Suzuki, R.; Sakano, M.; Zhang, Y.; Akashi, R.; Morikawa, D.; Harasawa, A.; Yaji, K.; Kuroda, K.; Miyamoto, K.; Okuda, T. *Nat. Nanotechnol.* **2014**, *9*, 611−617.

(19) Morin, S. A.; Bierman, M. J.; Tong, J.; Jin, S. *Science* **2010**, *328*, 476−480.

(20) Bierman, M. J.; Lau, Y. K. A.; Kvit, A. V.; Schmitt, A. L.; Jin, S. *Science* **2008**, *320*, 1060−1063.

(21) Zhu, J.; Peng, H. L.; Marshall, A. F.; Barnett, D. M.; Nix, W. D.; Cui, Y. *Nat. Nanotechnol.* **2008**, *3*, 477−481.

(22) Lee, Y. H.; Zhang, X. Q.; Zhang, W. J.; Chang, M. T.; Lin, C. T.; Chang, K. D.; Yu, Y. C.; Wang, J. T. W.; Chang, C. S.; Li, L. J.; Lin, T. W. *Adv. Mater.* **2012**, *24*, 2320−2325.

(23) van der Zande, A. M.; Huang, P. Y.; Chenet, D. A.; Berkelbach, T. C.; You, Y. M.; Lee, G. H.; Heinz, T. F.; Reichman, D. R.; Muller, D. A.; Hone, J. C. *Nat. Mater.* **2013**, *12*, 554−561.

(24) Najmaei, S.; Liu, Z.; Zhou, W.; Zou, X. L.; Shi, G.; Lei, S. D.; Yakobson, B. I.; Idrobo, J. C.; Ajayan, P. M.; Lou, J. *Nat. Mater.* **2013**, *12*, 754−759.

(25) Winer, W. O. *Wear* **1967**, *10*, 422−452.

(26) Wang, H. W.; Skeldon, P.; Thompson, G. E. *Surf. Coat. Technol.* **1997**, *91*, 200−207.

(27) Chhowalla, M.; Shin, H. S.; Eda, G.; Li, L. J.; Loh, K. P.; Zhang, H. *Nat. Chem.* **2013**, *5*, 263−275.

(28) Meyer, J. C.; Geim, A. K.; Katsnelson, M.; Novoselov, K.; Booth, T.; Roth, S. *Nature* **2007**, *446*, 60−63.

(29) Lauritsen, J. V.; Kibsgaard, J.; Helveg, S.; Topsoe, H.; Clausen, B. S.; Laegsgaard, E.; Besenbacher, F. *Nat. Nanotechnol.* **2007**, *2*, 53−58.

(30) Shen, Y. R. *The Principles of Nonlinear Optics*; J. Wiley & Sons Inc. Press: Hoboken, NJ, 2003.

(31) Lee, C.; Yan, H.; Brus, L. E.; Heinz, T. F.; Hone, J.; Ryu, S. *ACS Nano* **2010**, *4*, 2695−2700.

(32) Bollinger, M.; Lauritsen, J.; Jacobsen, K.; Nørskov, J.; Helveg, S.; Besenbacher, F. *Phys. Rev. Lett.* **2001**, *87*, 196803.

(33) Burton, W. K.; Cabrera, N.; Frank, F. C. *Philos. Trans. R. Soc., A* **1951**, *243*, 299−358.